The influence of fluvial incision on fault activities in the central segment of the Longmenshan thrust belt, eastern Tibetan plateau

Authors: Xibin TAN[1*], Han YUE[2], Yiduo LIU[3], Xiwei XU[1], Feng SHI[1], Chong XU[1], Zhikun REN[1], J. Bruce H. SHYU[4], Renqi LU[1], Haijian HAO[1]

1 Key Laboratory of Active Tectonics and Volcano, Institute of Geology, China Earthquake Administration, Beijing, 100029, China

2 School of Earth and Space Sciences, Peking University, Beijing, 100871, China

3 Department of Earth and Atmospheric Sciences, University of Houston, Houston, Texas, 77204-5007, USA

4 Department of Geosciences, National Taiwan University, Taipei, 106, Taiwan

(Submiited to *Tectonics,* on Oct 20, 2017.)

Abstract

Whether external or internal forces of the Earth control the behaviors of upper-crustal faults in a fold-and-thrust belt has been debated for decades. The Longmenshan thrust belt (LTB) along the eastern margin of the Tibetan Plateau may provide insights into such a debate. In this study, we focus on the central segment of the LTB which has relatively uniform shortening strains yet various fluvial incision capability along the strike. This tectonic setting enables a better assessment of the effects of external forces on fault activities. We analyzed the variations of the topography, fluvial incision intensity, co-seismic slips, and co-seismic landslides along the central LTB. The Longmen sub-segment in the northern half has higher elevation and three times lower fluvial incision intensity than the Hongkou sub-segment in the south. We calculated the topographic stresses on the faults ruptured during the 2008 Wenchuan earthquake and found topographic introduced normal stress increase may explain the co-seismic slip partitioning onto two sub-faults along the Longmen sub-segment. Our results indicate that fluvial incision may have produced the along-strike variations of the topography, which may further produce the different rupture behavior. In addition, the mean hillslope angle along the central LTB prior to the 2008 Wenchuan earthquake appeared to be at the

critical condition of this region. Co-seismic deformation reduced the mean hillslope angle significantly, indicating that geomorphic indices may vary with different stages in an earthquake cycle. Therefore, scrutinizing the mean hillslope angle and other geomorphic indices may help identify potential seismic hazards in an active fault system.

Keywords: Wenchuan earthquake, Longmenshan, fluvial incision, external forces, Tibetan Plateau

Introduction

The upper continental crust is a critical zone of interactions and competitions between internal and external geologic forces. Internal forces are manifested by deep, solid-state processes within the interior of the Earth, and are essentially energized by radiogenic heating through mantle convection between thermal boundary layers (e.g., Tackley, 2000; Jaupart et al., 2015). External forces, by contrast, operate on or around the Earth's surface, through fluvial, glacial, eolian, oceanic, and atmospheric processes, and they are primarily driven by solar radiation as well as the release of gravitational potential energy (e.g., Allen, 2009). While most studies focus on the effects of internal forces on crustal deformation, scientists are paying increasing attentions to the roles of external forces, particularly erosion, in upper-crustal deformation in recent decades (Molnar and England, 1990; Avouac and Burov, 1996; Willett, 1999; Beaumont et al., 2001; Zeitler et al., 2001; Steer et al., 2014; Zhang et al., 2016). Using topographic observations, analytical and numerical modeling techniques, and analog experiments, substantial studies have shown that erosion strongly influences on, or even controls crustal deformation, especially along fold-and-thrust belts (e.g. Dahlen and Suppe, 1988; Beaumont et al., 1992; Avouac and Burov, 1996; Mugnier et al., 1997; Willett, 1999; Steer et al., 2014;). In local studies, nevertheless, it is often difficult to identify whether the internal or external forces dominate, which usually raises the "chicken-versus-egg" controversy (e.g. Molnar and England, 1990; Wang et al., 2014; Zeitler et al., 2015).

The Longmenshan thrust belt (LTB) along the eastern margin of the Tibetan Plateau is of particular interest in seismic and tectonic studies, due to the catastrophic 12 May 2008 M_w 7.9 Wenchuan earthquake (Fig. 1). Abundant new data and insights have been obtained from various disciplines including seismology, geodesy, structural geology, thermochronology, and

geomorphology (e.g. Xu et al., 2009; Shen et al., 2009; Zhang et al., 2012; and many others). Among these studies, a key issue is to identify the dominating mechanism of the LTB's crustal deformation; that is, whether it is the external or the internal forces that primarily determine the fault characteristics and activities. High relief, active thrust faults, and thickened, partially molten lower crust of the LTB demonstrate the ongoing contractional forces within the interior of the Earth in this region (e.g. Zhang et al., 2010; Lu et al., 2014). Previous studies also highlighted the relationships between the topography and fault activities by lateral comparison between the northern, central, and southern segments of the LTB (Zhang et al., 2011; Gao et al., 2016; Sun et al., 2016) (Fig. 1). However, the "chicken-or-egg" debate still holds due to the lack of a "control group" in these studies, because both the landscape and total shortening strains vary, sometimes significantly, amongst the segments of LTB, which weakens the argument for or against either mechanism (Godard et al., 2009, 2010; Wang et al., 2012; Tan et al., 2017a, 2017b). In fact, a large spatial scale tends to reduce the consistency of both the external and internal forces, particularly the latter one, because of the structural and mechanical heterogeneities within the crust. To evaluate the impact of external forces, one would ideally attempt to eliminate the influence of internal forces by selecting tectonically similar domains with varied surficial processes along-strike.

The central segment, instead of the entire LTB, provides a better test ground for this purpose, because: (1) the Pengguan massif that occupies the backbone of the central LTB is not pervasively fractured and probably remains cohesive (Fig. 2); (2) the timing and amount of exhumation of the Pengguan massif show small along-strike difference (Godard et al., 2009; Wang et al., 2012); and (3) the total co-seismic slips are essentially identical along strike within the central segment (Xu et al., 2009; Shen et al., 2009) (Fig. 1). Overall, the along-strike variation of the internal forces within the central LTB is minor. By contrast, the along-strike variation of fluvial incision intensity is significant (Godard et al., 2010). Therefore, we infer that the external forces play a dominant role for the along-strike variation of fault activities along the central segment of LTB. To test this hypothesis, in this paper, we examined the along-strike variations of the topography, fluvial incision intensity, co-seismic slips, and landslides triggered by the 2008 Wenchuan earthquake along the central segment of the LTB, modeled the influence of the topography on the compressional normal stress on fault planes, and analyzed the influence and significance of fluvial incision on the faulting processes along active thrust belts.

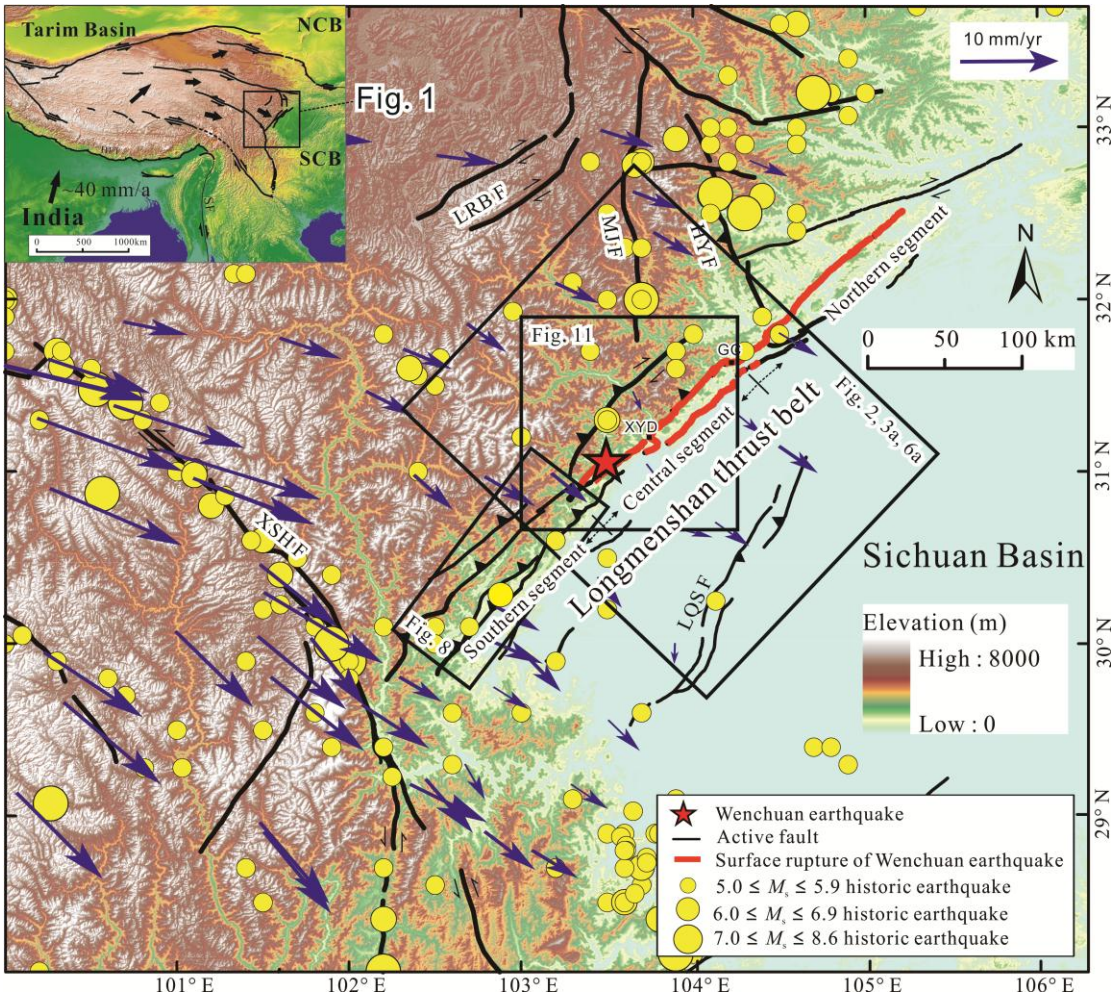

Figure 1. Map of the active tectonics and topography of the Longmenshan region along the eastern margin of the Tibetan Plateau. Insert map shows the tectonic boundaries and major faults in and around the Tibetan Plateau. Epicenter and surface ruptures of the 12 May 2008 M_w 7.9 Wenchuan earthquake from Yu et al. (2010). GPS data (blue arrows) from Liang et al. (2013). Boxes show the extents of Figs. 2, 3a, 6a, 8, and 11. Abbreviation: MJF, Mingjiang Fault; XSHF, Xianshuihe Fault; HYF, Huya Fault ; XYD, Xiaoyudong step-over; GC, Gaochuan step-over; LQSF, Longquanshan Fault ; NCB, North China Block; SCB, South China Block.

Geological Background

The LTB is a northeast-trending structure (500 km-long, and 30-60 km-wide) which defines the boundary between the eastern Tibetan Plateau and the Sichuan Basin (Fig. 1). Within 50 km of distance across the LTB, the mean elevation ascends dramatically from ca. 500 m above sea level

in the Sichuan Basin to over 5000 m in the Tibetan Plateau, forming the steepest topographic gradient in the Tibetan Plateau region and, arguably, of the world (Fig. 2; Kirby et al., 2002; Clark and Royden, 2000). The LTB is divided into the northern, central, and southern segments based on fault activity and surface geology, (Fig. 1; Zhang et al., 2011). The 12 May 2008 M_w 7.9 Wenchuan earthquake ruptured the central and northern segments of the LTB (e.g., Xu et al., 2009). GPS measurements show horizontal shortening rates are less than 3 mm/yr across the LTB (King et al., 1997; Chen et al., 2000; Gan et al., 2007; Zheng et al., 2017).

The LTB is also a major boundary between lithospheric units. Songpan-Ganzi terrane northwest of the LBT is characterized by Triassic clastic sedimentary rocks in a deep-water turbiditic depositional environment and slope-facies flysch, and a long-lived intracontinental orogenic belt since the Mesozoic (e.g., Roger et al., 2010). The Sichuan Basin to the southeast is part of the Yangtze craton, which has been mostly stable since the Proterozoic, a survivor of multiple supercontinental cycles and mantle plumes (Li et al., 2007; Xu et al., 2004).

The central segment of LTB contains three major faults, namely, from west to east, the Wenchuan-Maoxian fault, Beichuan-Yingxiu fault (BYF), and Jiangyou-Guanxian fault (JGF) (Figs. 1&2). They are NW-dipping, SE-vergent, imbricated thrust faults with a generally foreland-ward propagation history based on seismic- and field-based analyses and low-temperature thermochronology (Hubbard and Shaw, 2009; Lu et al., 2014; Tan et al., 2017). Surface exposures consist of predominantly Precambrian crystalline basement rocks (the Pengguan massif and Xuelongbao massif in the central LTB) as well as Paleozoic marine sedimentary sequences (Fig. 2; Liu et al., 1996; Ma and Yang, 2001). The Wenchuan-Maoxian fault juxtaposes the Xuelongbao massif in its hanging-wall block against the Pengguan massif in the footwall block. To the east, the BYF carries the Pengguan massif and Paleozoic sedimentary rocks over Mesozoic strata. The JGF and its splay faults form the boundary between Paleozoic marine sediments and Cenozoic and Cretaceous sediments in the Sichuan Basin (Lu et al., 2012). The Wenchuan earthquake was accompanied by ~240 and ~70 km long surface ruptures along the BYF and the JGF, respectively (Fig. 1) (e.g. Xu et al., 2009; Yu et al., 2010). These two faults show dextral-thrust and thrust movements, respectively.

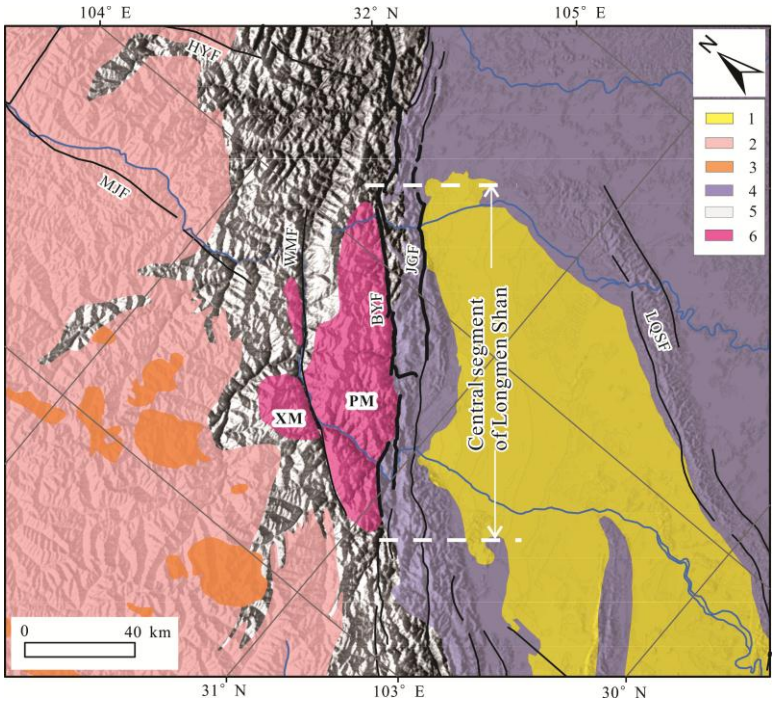

Figure 2. Geologic map of the central Longmenshan and surrounding areas. Numbers and abbreviations: 1, Cenozoic; 2, Triassic flysch; 3, Mesozoic granite; 4, Mesozoic sedimentary rocks; 5, Paleozoic metamorphic rocks; 6, Pre-Cambrian igneous and metamorphic rocks; BYF, Beichuan-Yingxiu fault; JGF, Jiangyou-Guanxian fault; LQSF, Longquanshan fault; MJF, Mingjiang fault; WMF, Wenchuan-Maoxian fault; PM, Pengguan massif; XM, Xuelongbao massif.

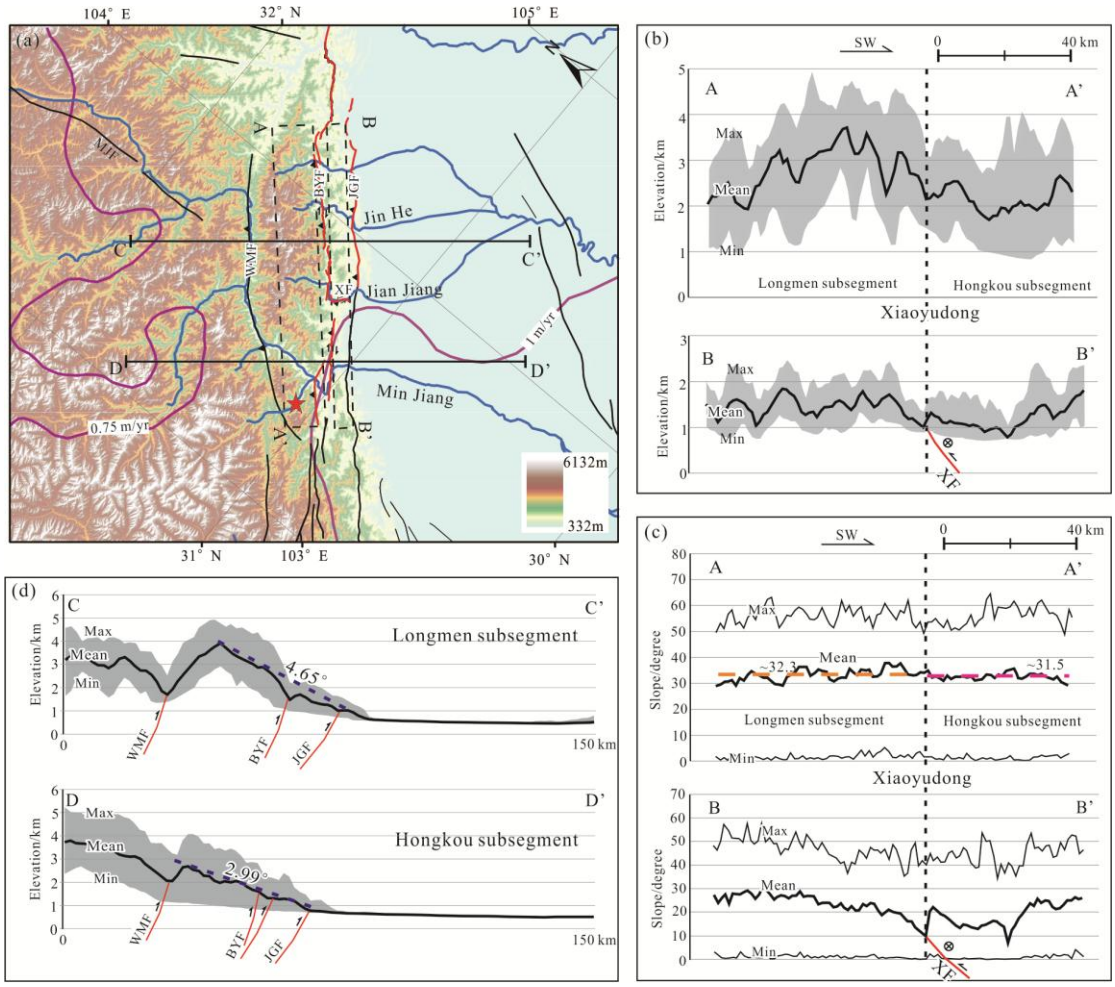

Figure 3. Along-strike variations of topography in the central Longmenshan. (a) Map of the topography of the central LMS. Black line, active fault; red line, surface rupture of the 2008 Wenchuan earthquake; blue line, river; purple line, precipitation contour. (b) Topographic relief along swath profiles AA' and BB'. (c) Slope distribution along swath profiles AA' and BB'. (d) Topographic relief along profiles CC' and DD', which outline a swath of 30 km wide along CC' and DD', respectively. For each profile, three curves (mean, maximum, and minimum) are plotted against the distance.

Along-strike variations in the central LTB

The central segment of LTB can be further divided into the Longmen sub-segment (LMSS) and the Hongkou sub-segment (HKSS), to the north and south of the Xiaoyudong area, respectively (Fig. 3) (Yu et al., 2010). In this chapter, by re-visiting published data, we quantify the differences between the two sub-segments in terms of the topography (Jarvis et al., 2008), fluvial incision

intensity (Godard et al., 2010), co-seismic slip (Shen et al., 2009), and landslides triggered by the 2008 Wenchuan earthquake (Xu et al., 2014).

Topography

We used the SRTM 90-m resolution digital elevation model (DEM) (Jarvis et al., 2008) as raw data, to analyze the elevation-slope variations along the central LTB using ESRI ArcGIS® and Microsoft Excel® software. Three toolsets are used in ArcGIS®: Divide, Buffer, and Zonal Statistics as Table.

Figure 3 illustrates the topographic variations in the study area. Two swaths, AA' (20 km wide) and BB' (14 km wide), are placed along the hanging-wall and footwall blocks of the BYF, respectively (Fig. 3a). Elevation is plotted against its location along each swath with the mean, maximum, and minimum values, as shown in Fig. 3b. Similarly, the slope of each pixel of the DEM (90 m by 90 m), calculated from the Slope function in ArcGIS, is also plotted against the length along the two swaths, with the mean, maximum, and minimum slope curves (Fig. 3c). The Xiaoyudong fault is displayed on the BB' profiles as the border between the two sub-segments, showing sinistral reverse motion. Profiles CC' and DD' are along the normal direction of the central LTB, across the LMSS and HKSS, respectively (Fig. 3a). The elevation profiles of CC' and DD' are generated from all pixels within 15 km distance of each transect line, with the mean, maximum, and minimum value curves (Fig. 3d).

Topographic differences exist between the two sub-segments of the central LTB, as shown in Fig. 3b & 3c. In the hanging-wall block of the BYF (profile AA', Fig. 3b), the mean elevation is 2.81 ±0.48 km (1σ, same below) north of Xiaoyudong, whereas it is only 2.12 ±0.26 km in the south. In the footwall block of the BYF, similarly, the mean elevation of the LMSS (1.44 ±0.19 km) is also higher than that of the HKSS (1.16 ±0.24 km). In addition, compared with the HKSS in the south, the LMSS shows a stronger fluctuation of the elevation along its strike.

Slopes of the topography do not vary as much as the elevation along profile AA' (Fig. 3c). The LMSS has a mean slope of 32.3 ±2.3 °, and the HKSS 31.5 ±2.3 °, which are essentially undiscernible. By contrast, slopes differ along the profile BB' in the footwall of BYF: the mean slopes are close to 30 ° towards both ends, whereas it is generally less than 20 ° around the Xiaoyudong fault in the

178 middle of the profile.

179

180 **Fluvial incision intensity**

181 We evaluated the intensity of fluvial incision and its relations with the topography in the central
182 LTB. Currently, models proposed for the evolution of river beds can be classified into two families:
183 the detachment-limited models (Howard et al., 1994), and the transport-limited models (Whipple
184 and Tucker, 2002). Despite large differences in behavior, higher fluvial shear stress on the bottom
185 of a channel qualitatively corresponds to higher erosion capacity of the river, in both end-member
186 formulations. Therefore, the fluvial shear stress is usually treated as a proxy for incision intensity
187 (Godard et al., 2010), and it is defined as

188 $\tau = \rho g R S$ （1）

189 where ρ is the water density, g is the gravitational acceleration, R is the hydraulic radius and S is the
190 stream slope. For streams with large width-to-depth ratio, R is close to the flow depth H. Using the
191 depth-averaged flow velocity U, through mass conservation and the Manning's equation, the shear
192 stress can be recast as a function of channel slope S and water discharge Q,

193 $\tau = \rho g (Q \cdot N)^{3/5} S^{7/10} W^{-3/5}$ （2）

194 where W is the channel width, and N is the channel roughness (Godard et al., 2010).

195 From Eq. (2), Godard et al. (2010) computed the fluvial shear stress profiles along three rivers,
196 the Min Jiang, the Jian Jiang and the Jin He, as shown in Figure 4. The fluvial shear stress in the
197 hanging-wall of the BYF along the Min Jiang has an average of ~400 Pa, which is almost 3 times
198 as much as those along the Jian Jiang and the Jin He (~150 Pa). Such differences show a stronger
199 fluvial incision intensity of the Min Jiang in the HKSS than that of the Jian Jiang and the Jin He in
200 the LMSS. In general, areas with stronger fluvial incision intensity tend to produce lower topography,
201 assuming the same rock uplift rate. The difference of the fluvial incision intensity among these rivers,
202 therefore, shows a correlation with the topographic variations shown in profile AA'.

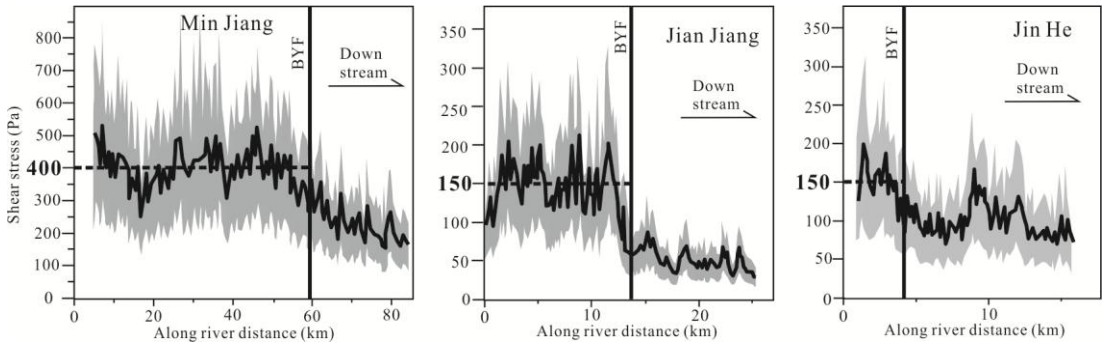

Figure 4. Shear stress profiles (black curves) along the rivers with cumulative uncertainties (grey areas) (revised from Godard et al., 2010). Note the different scales of vertical axes (shear stress, in Pascal) between Min Jiang and the other two rivers.

Co-seismic thrust slip of the 2008 Wenchuan earthquake

Seismological studies show that the mainshock of the 12 May 2008 Wenchuan earthquake sourced on the BYF about 30 km southwest of the town of Yingxiu, and propagated unilaterally northeastward (Wang et al., 2008; Shen et al., 2009). Surface ruptures are found along both the BYF and JGF along the central segment of the LTB, based on field investigations and detailed mappings of post-earthquake satellite images (Fig. 3a) (Xu et al., 2009; Liu-Zeng et al., 2009; Yu et al., 2010). The Xiaoyudong rupture zone, a short, northwest-striking fault zone, links the two major rupture zones at the southern end of the JGF through an oblique ramp (Fig. 3a). The BYF branches into two strands east of the town of Yingxiu, where the primary fault strand strikes southwest and the other west through Yingxiu. Both strands ruptured in the 2008 Wenchuan earthquake (Fig. 3a).

Shen et al. (2009) inverted GPS and Interferometric Synthetic Aperture Radar (InSAR) data to infer the fault geometry and slip distributions associated with the earthquake. From Yingxiu to Xiaoyudong of the HKSS, the BYF shows high fault-slips at 0-10 km depth with 5 m of thrust slip on average (Fig. 5). In the LMSS, the BYF displays moderate thrust slip of 2-4 m. The PGF accommodates moderate amounts of slip (ca. 1.5 m on average) in the northeast of Xiaoyudong, whereas no slip is observed on the PGF in the HKSS (Fig. 5). The inverted results of the co-seismic slip are consistent with co-seismic displacements of surface ruptures measured in the field (blue lines in the Fig. 5) (Xu et al., 2009; Liu-Zeng et al., 2009; Yu et al., 2010).

In brief, an obvious difference of co-seismic thrust slip behavior exists between the LMSS and HKSS: slip is concentrated on the BYF in the HKSS south of Xiaoyudong, whereas it is partitioned

onto the BYF and JGF in the LMSS. The total slips in both sub-segments are similar, and the conjugate Xiaoyudong fault in the middle may play important roles in the strain partitioning.

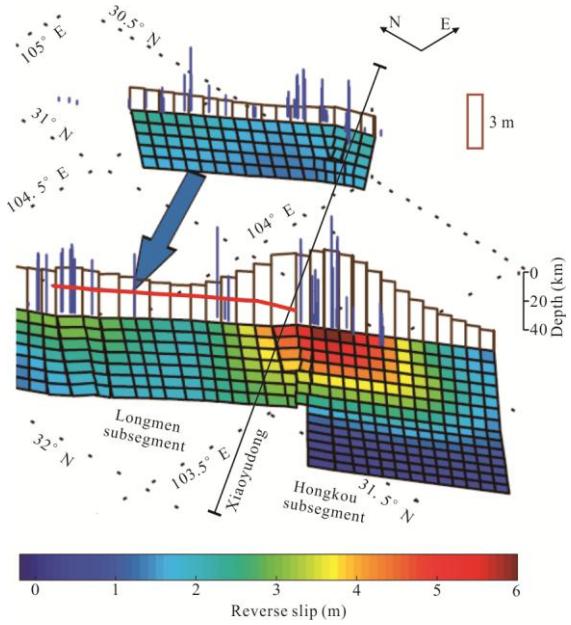

Figure 5. Co-seismic thrust slip of the 2008 Wenchuan earthquake at the central segment of Longmenshan fault belt. Revised from Shen et al. (2009).

Landslides triggered by the 2008 Wenchuan earthquake

Besides the co-seimic slip along the LTB, another significant geological phenomenon is the massive landslides caused by ground shaking during the Wenchuan earthquake. The earthquake triggered an immense number of landslides (Parker et al., 2011). More than 200,000 landslides were documented in the most detailed and complete landslide database related to the earthquake (Xu et al., 2014). Figure 6 shows the distribution of co-seismic landslides along the central segment of LTB. We choose a swath (110 km long and 10 km wide, outlined by EE') in the hanging-wall block of the BYF in the central LTB, to conduct a statistical analysis of the landslides. The total number of landslides in this swath is 44,138 with a total area of 288.5 km^2 and total volume of 2.996 km^3.

In order to assess whether and how landslide distribution varies along-strike, we broke down our sampling swath into 110 rectangles along its length, and calculated the amount, area, and volume of landslides in each of the 10 km by 1 km rectangles (Xu et al., 2016). In spite of the contrast on the average amount of co-seismic landslides between the northern and southern sub-segments (ca. 318 and 517, respectively), the mean area and volume of the two groups are highly similar. This

implies that co-seismic landslides in the hanging-wall block of the BYF are comparable in their total area and total volume between the two subsegments of the central LTB. Also, statistical results of the landslide volumes suggest an average of 2.7 m (i.e., the mean volume, ca. $2.7\times10^7 m^3$, divided by area, 1×10^7 m^2, in each rectangle) slip along the profile EE' caused by the Wenchuan earthquake (Fig. 6c).

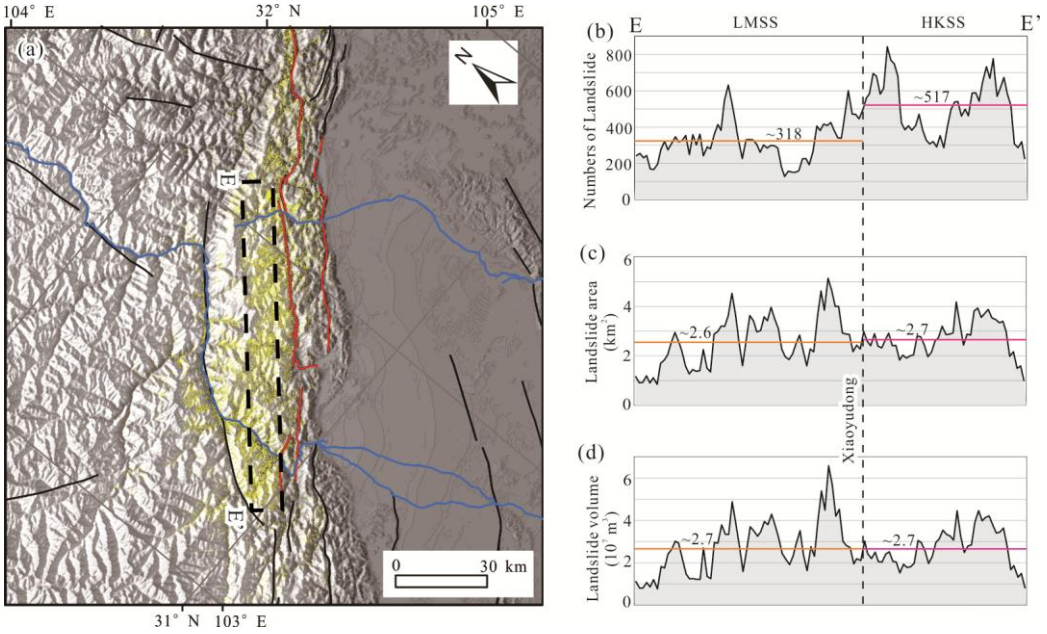

Figure 6. Co-seismic landslides in the central LMS. (a) Distribution of the landslides (yellow polygons) in the central LMS (data from Xu et al., 2014), plotted on the digital elevation model of this region. Also shown are the major rivers (blue), active faults (black), and surface ruptures of the Wenchuan earthquake (red). (b) The number of co-seismic landslides in each sampling window (10 km by 1 km rectangle) along profile EE'. (c) The area of co-seismic landslides in each sampling window along EE'. (d) The volume of landslides in each rectangle along EE'. Orange and pink lines show the mean value of the Longmen and Hongkou sub-segments, respectively.

Influence of topographic weight on reverse faulting

The absolute stress status near an active fault is composed of tectonic-loaded stress, topographic stress, compensated stress and seismic/aseismic released stress (Luttrell et al., 2011; Styron and Hetland, 2015). Computing the full stress status relies on knowledge of stress accumulation and releasing history during earthquake cycles and influences of isostatic compensation and lower crust relexations, which is not available for the Wenchuan area. However, the topographic stress can be estimated from the topography data. Such strategy was adopted by Styron and Hetland (2015) to estimate the background stresses near the Wenchuan earthquake source area. In this study, we adopted the Boussinesq assumption (Liu, 1992; Styron and Hetland, 2015) by which the topographic stresses are estimated as a response of vertical stress loading on the ground surface. The Boussinesq assumption is a first-order approximation enabling a preliminary quantitative estimation. We divided the topographic data into 90m*90m grids and compute the stress tensor field (stress kernels) in response to a unit point surface loading. Stress kernels are computed at each depth from 1 to 20 km with 1 km increment and convolved with the topography data to computed full stress tensor field at each depth. We used the fault geometry from Wan et al. (2016) and interpolated stress tensors on each subfault. Normal and shear tractions are projected to the subfault normal direction using the geometry of each sub-fault in order to compute normal and shear tractions on the fault plane (Fig. 7). In this study, we mainly considered the compressional stresses in the fault normal direction as a stress barrier, with a similar logic as that adopted in the analysis of the 2016 Kumamoto earthquake (Yue et al. 2017).

Normal stress on the two faults and along swath profiles CC' and DD' are computed and plotted in Figure 7. Normal stresses on the fault plane are calculated with respect to the plane geometry of each individual sub-fault, whereas the normal stresses along the two profiles are computed referenced to the averaged fault orientation (strike = 226 °, dip = 65 °, right-hand rule) of the major fault planes. Normal stresses on the major fault plane (i.e., BYF) are found to be significantly higher (~1 MPa) along profile CC' than that along profile DD'. Such significant normal stress increase is introduced by the higher topography above the BYF along CC' swath profile (Fig. 7b): a lobe of normal stress increase is caused by the mountain weight and projected to the BYF.

The normal stress distribution also appears to be anti-correlated with the co-seismic slip pattern on the main fault plane (BYF), by which the mean slip along profile DD' (~5 m) is larger than that along profile CC' (~3 m). Along profile CC' co-seismic slip is allocated as 2-3 m of slips on both the BYF and JGF, yielding comparable cumulative slips as that along profile DD'. Normal compressional stresses on the JGF (CC') is comparable to that on the BYF along profile DD', which indicates the dynamic rupture prefers to occur on a less compressed fault segment. The high compressional stress on the BYF near the CC' profile appears to work as a stress barrier that prohibits the dynamic rupture on the BYF. This is consistent with the mechanism revealed by the sandbox experiment (Sun et al., 2016) and the Late-Cenozoic evolution of the thrust belts (Tan et al., 2017a), yet the co-seismic slip partitioning is a new insight revealed by the Wenchuan earthquake. The above analysis indicates the higher topography along profile CC' may function as a stress barrier that promotes the dynamic slip partitioning on a secondary fault plane.

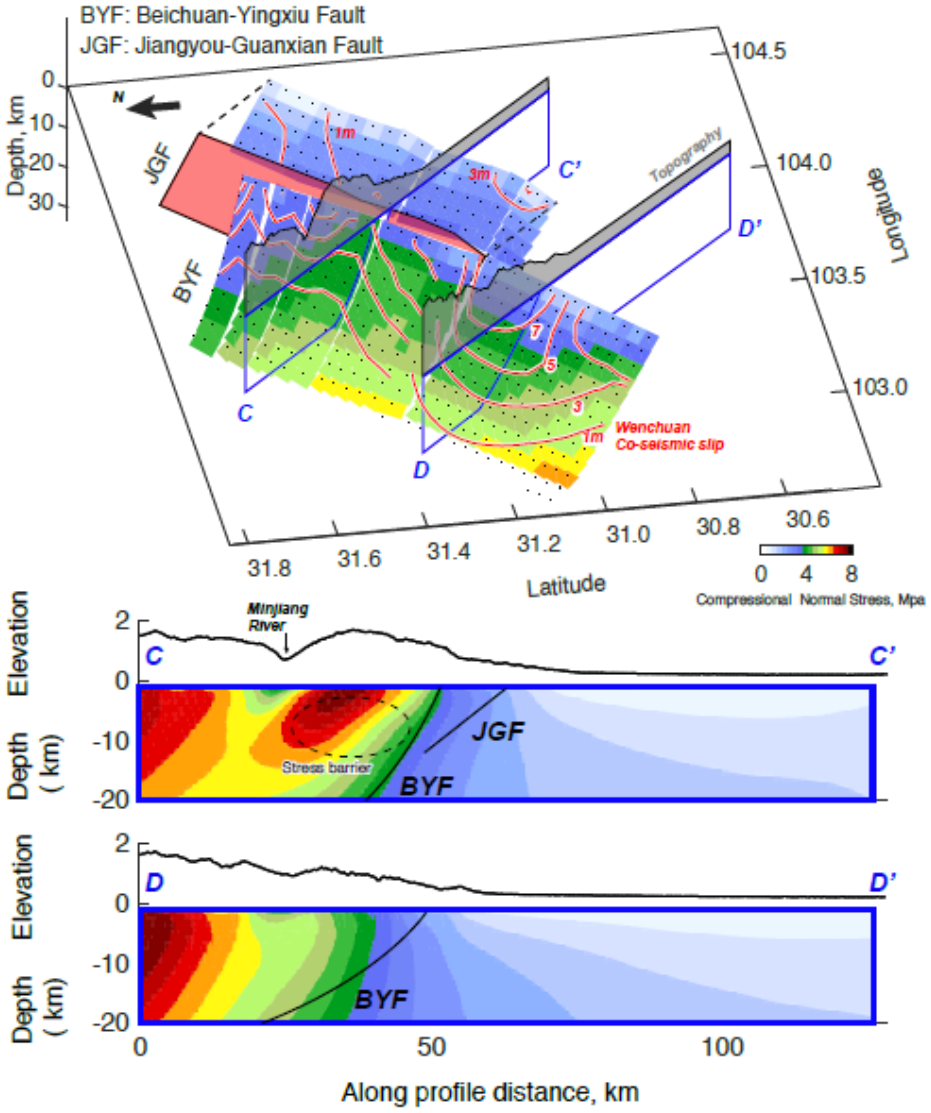

Figure 7. Calculations of compressional normal stress on fault surfaces. (a) Configurations of the Beichuan-Yingxiu and Jiangyou-Guanxian faults in the model. Fault geometry from Wan et al. (2016). Contours of co-seismic slips of the Wenchuan earthquake shown in red. Locations of CC' and DD' are same as Fig. 3. (b) Resolved distribution of compressional normal stresses on two transects CC' and DD'.

Discussions

Mechanism for the along-strike variations in central LTB

As presented above, topographic variations can influence the normal stresses on major fault surfaces. Compared with the HKSS, the higher topography in the LMSS causes stronger normal

316 stresses on the BYF (Fig. 7), which increases the friction along this sub-segment (given a uniform
317 coefficient of internal friction in the central LTB, Dahlen et al., 1984). Since it is not favorable to
318 accommodate the strains solely on the BYF, thrust slips are thus partitioned onto the JGF in the
319 LMSS, resulting in the long-term activity of the JGF and greater amount of co-seismic total slip in
320 the LMSS than the HKSS during the 2008 Wenchuan earthquake (Lu et al., 2014; Tan et al., 2017a).
321 Therefore, the topographic variations in the hanging-wall block of the BYF play a major role in
322 producing the fault activity and co-seismic slip differences between the LMSS and HKSS. A
323 question is thus raised: how is the along-strike variation of the topography formed?

324 It is a classical conception in geomorphology that landscapes result from an interaction
325 between internal tectonic processes and external denudation processes (e.g. Willett and Brandon,
326 2002; Whipple and Meade, 2004; Godard et al., 2010). Therefore, two possible scenarios exist to
327 produce the along-strike variations of the topography: (1) thrust faulting in the LMSS is stronger
328 than that in the HKSS, or (2) the erosion is weaker in the LMSS than the HKSS.

329 Both mechanisms work for profile BB'. Nevertheless, the former one violates the geological
330 observations along profile AA', as the amounts of co-seismic slip and denudation in the LMSS is
331 no greater than those in the HKSS (Xu et al., 2009; Shen et al., 2009; Godard et al., 2009; Wang et
332 al., 2012). This mechanism can thus be ruled out. The latter mechanism can readily explain the
333 observations. Along-strike variations of the topography result from different fluvial erosion
334 intensities, under the circumstances in which precipitation, lithology, and co-seismic landslides
335 show little differences between the two sub-segments (Figs. 1, 2, and 6). In fact, the Min Jiang which
336 runs through the HKSS bears greater fluvial erosion intensity than the other two rivers (Fig. 3).
337 Therefore, fluvial erosional processes or broadly the external forces appears to control the
338 topographic variations, which further play a critical role in defining the stress status and behaviors
339 of the fault system in the central LTB.

340

341 **Topographic influence on co-seismic slip and orogenic development**

342 The initial dynamic rupture of the 2008 Wenchuan earthquake was located in a relatively low-
343 elevation area southwest of the town of Yingxiu (Fig. 3). Co-seismic surface rupture propagated
344 predominantly to the north where the topography is low and only slightly to the south where high
345 mountains are present (Fig. 8) (Wang et al., 2008; Shen et al., 2009). Similar to the 2008 Wenchuan

346 earthquake, the 20 April 2013 M_w 6.6 Lushan earthquake also ruptured the low-elevation area first
347 (Fig. 8), but its subsurface ruptures propagated bilaterally for 20-30 km (Wang et al., 2013; Jiang et
348 al., 2013). Landscape between the epicenters of these two earthquakes is characterized by high-
349 elevation mountains (Fig. 8). According to the numerical modeling above, high topography can
350 obstruct the propagation of co-seismic slip. This phenomenon is also observed in the 2016
351 Kumamoto M_w7.0 earthquake: surface rupture initiated in the low-elevation area, propagated
352 northeastward, and terminated at the Aso caldera which is about 1 km higher than other ruptured
353 region. The topography-induced stress barrier is considered as a possible mechanism for the
354 dynamic rupture termination (Yue et al., 2017).

355 High topography-derived excess load can affect not only the co-seismic slips on major thrusts,
356 but also the development of contractional orogens. Bollinger et al. (2004) showed that the loading
357 of the high Himalayan massifs increased the normal stress suppressed the microseismicity and
358 increased fault locking on the Main Himalayan Thrust. Meade and Conrad (2008) demonstrated that
359 the increased weight of the uplifting Andes influenced the Nazca-South America convergence rate.
360 Results from sandbox modeling also suggests that the topography casts influences on the rate of
361 thrust fault propagation towards the foreland in the LTB (Sun et al., 2016). Our analysis further
362 demonstrates that the along-strike variations of topography influenced the fault activities and,
363 subsequently, the orogenic processes in the central LTB. Given similar boundary conditions from
364 the interior of the Earth, intense fluvial incision can reduce the elevation, leading to a more stable
365 Coulomb wedge, and thus shortening strain tends to be accommodated by existing major thrust
366 faults. By contrast, weaker fluvial incision is not efficient enough to denude the surface, therefore
367 it is easier to reach the critical state in the Coulomb wedge, causing the propagation of faults toward
368 the foreland with the locking of existing thrust faults.

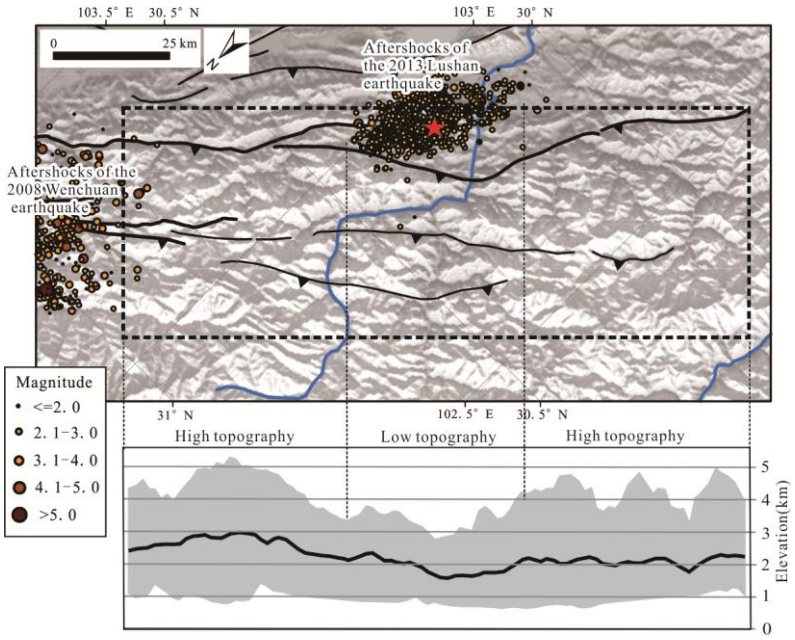

Figure 8. Distribution of the aftershocks of the 2008 Wenchuan earthquake and the 2013 Lushan earthquake, and the topographic variations along the central and southern segments Longmenshan.

The topographic evolution in an earthquake cycle and its implications

Quantitative topographic analysis has been increasingly used in active tectonic researches since two decades ago, thanks to the advances of the DEM technology (e.g. Burbank et al., 1996; Kirby et al., 2008; Zhang et al., 2011; Chen et al., 2016). In their hillslope analysis in the western Himalayan syntaxis, Burbank et al. (1996) found that the average angles of hillslopes (~32 ±2 ° for 270-m windows) are steep and essentially independent of the erosion rate but controlled by a common threshold process. Kirby et al. (2003) suggested relatively high uplift rates in southern and central LTB, based on the distribution of rock uplift inferred from channel profile steepness.

Recent improvements of the DEM resolution lead to the findings that in tectonically active areas, a strong earthquake and its associated co-seismic landslides result in a sudden pulse in landscape evolution, as shown by geomorphological indices (e.g. Oskin et al., 2012; Ren et al., 2014). Unexceptionally, the 2008 M_w7.9 Wenchuan earthquake dramatically modified the topography of the Longmenshan region by regional uplift and massive landslides (Xu et al., 2009, 2014; Parker et al., 2011). Prior to the 2008 Wenchuan earthquake, the two sub-segments along profile AA' had almost identical mean hillslope angle (32.3 ±2.3 ° for the LMSS and 31.5 ±2.3 ° for the HKSS). Although the threshold strength of hillslopes within the Longmenshan mountain is

unknown, these values are highly similar to the threshold hillslopes (32±2°) of the Nanga Parbat/Haramosh area, and both regions have similar lithology in the bedrocks (i.e., metamorphic and igneous rocks) (Burbank et al., 1996; Zhang et al., 2011). Therefore, we infer that the mean hillslope of the central LTB may have reached the threshold when the Wenchuan earthquake occurred. This inference also explains why the LMSS and HKSS share comparable volume of co-seismic landslides. By comparing the geomorphic features before and after the earthquake, Ren et al. (2014) revealed that the Wenchuan earthquake smoothed the steep relief: the number of intermediate-relief area increased, whereas high-relief areas shrank (Fig. 9). According to the critical wedge theory (Davis, 1990), the hillslope angles will climb again and reach the threshold value when the next earthquake strikes the ground. Therefore, elucidating how geomorphology evolves at different stages during the earthquake cycle is of strong importance for seismic hazard assessment.

The Wenchuan earthquake altered the landscape in the central LTB moderately to markedly, which enables us to quantitatively characterize the development of geomorphic indices in the earthquake cycle using an integration of multiple types of data, including pre-earthquake geomorphic indices, co-seismic deformation, co-seismic geomorphic indices (Xu et al., 2009; Shen et al., 2009; Parker et al., 2011; Xu et al., 2014; Ren et al., 2014), and fluvial incision intensity and transportation ability (Godard et al., 2010; Liu-Zeng et al., 2011; Wang et al., 2017). Figure 10 illustrates the geomorphic evolution of the central LTB, in terms of the mean hillslope angle in an earthquake cycle: (1) Prior to the earthquake (such as the 2008 Wenchuan event), the hillslope angle of the hanging-wall block of the thrust (i.e., the Pengguan massif) reaches the critical value. (2) As the earthquake shakes and ruptures the ground, the Pengguan massif is uplifted while the mean angle of hillslope is reduced through co-seismic landslides. (3) Rivers transport the landslide deposits out of the thrust wedge after the earthquake event. (4) Following the transport, the rivers incise into the bedrocks, which steepen the mean hillslopes. (5) Finally, the mean hillslope angle reaches the threshold again, and a new earthquake cycle begins. For the central LTB, paleoseismology studies revealed an earthquake recurrence interval of ca. 3000 year in each segments (Ran et al., 2010; Chen et al., 2013; and Ran et al.'s unpublished data on the JGF). Therefore, we speculate that surface ruptures may occur again on multiple segments when next earthquake hits (Fig. 10b).

Differences of landscape evolution between the two sub-segments emerge in the earthquake

cycle. Along profile AA', both the HKSS and LMSS reached the critical mean angle of hillslope prior to the Wenchuan earthquake. Then, similar amounts of co-seismic landslides volume per unit area were produced in both sub-segments, as triggered by the Wenchuan earthquake (Xu et al., 2014). Consequently, similar mean angles of hillslope were attained immediately after the earthquake (Fig. 10b). The two numbers would start to diverge at stage (3) and the divergence would increase during stage (4), as the fluvial incision intensity is markedly different between sub-segments. Therefore, the HKSS with greater fluvial incision intensity would reach the critical mean angle of hillslope before the LMSS. It is still enigmatic how and why the HKSS could stay at the critical state of hillslope angles longer than the LMSS, if the recurrence intervals of the two sub-segments are similar. One possibility is that the HKSS actually has a shorter earthquake recurrence interval, which further raises the seismic risk of this region and demands more comprehensive research. It is also possible that the mean angle of hillslope is not the most direct proxy that accompanies the earthquake cycle. Future studies may find additional geomorphic indexes that are more sensitive to the development of critical tapers.

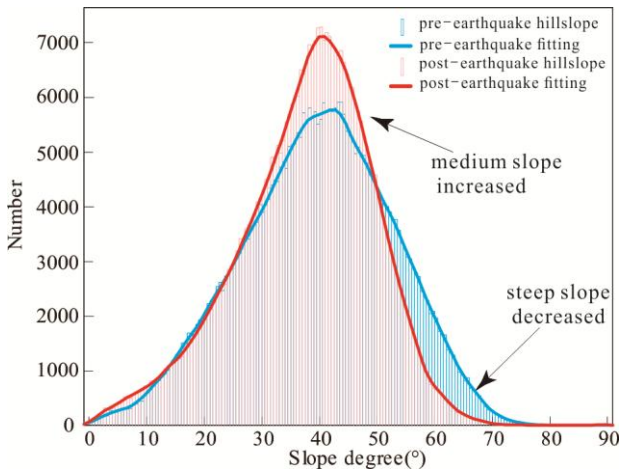

Figure 9. The distributions of hillslope angle immediately before (blue) and after (red) the 2008 Wenchuan earthquake. The histograms are fitted with smooth curves. The proportion of intermediate hillslope angles increased significantly after the Wenchuan earthquake, whereas the amount of steep slopes decreased. Revised from Ren et al. (2014).

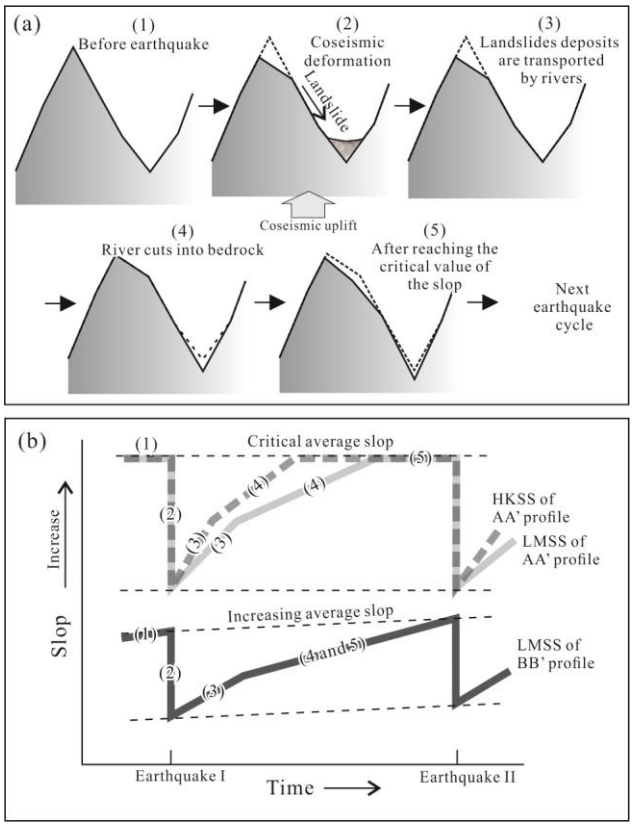

Figure 10. (a) Schematic diagrams of the landscape evolution during an earthquake cycle. (b) The evolution of hillslope angles that correspond to the different stages within the earthquake cycle. Note the differences between the LMSS and HKSS.

The NW-trending aftershock belt and the Xiaoyudong fault

A NW-trending belt of aftershocks is discovered to the west of Xiaoyudong (e.g., Huang et al., 2008; Wu et al., 2009) (Fig. 11). The strong ones (M_w > 5) on this aftershock belt show predominant left-lateral strike-slip focal mechanisms on NW-striking nodal planes (Fig. 11) (Hu et al., 2008; Wu et al., 2009; Hua et al., 2009; Cui et al., 2011; Yi et al., 2012). Therefore, the NW-trending belt of aftershocks may play a role of boundary between the LMSS and HKSS and adjust their differential fault activities (Fig. 11b).

Further to the northwest along the aftershock belt, the Miyaluo fault is exposed (Fig. 11). It displays sinistral sense of slip with unknown slip rates and has been inactive during the Holocene (Wang et al., 2015). The aftershock belt seems to be the southeastern extension of the Miyaluo fault, indicating that the Miyaluo fault may have been reactivated, and lateral propagation is taking place

in subsurface from the Tibetan Plateau towards the foreland. The NW-trending aftershock belt could also be an isolated, newly-formed fracture that would propagate towards and might link with the Miyaluo fault in the future. In either case, this aftershock belt can be regarded as a growing tear fault that accommodates the difference of fault-slips on the BYF between the LMSS and HKSS (Fig. 5), which matches its sinistral sense-of-slip (Fig. 11). More work is needed to better understand the NW-trending aftershock belt and its potential relations with, and seismic hazards along the Miyaluo fault.

The Xiaoyudong fault is an enigmatic secondary structure in the central LTB that marks the boundary between the two sub-segments (Fig. 11) (Li et al., 2009; Tan et al., 2012, 2017; Chang et al., 2012; Liu-Zeng et al., 2012; Sun et al., 2016). The 8-km long fault generally strikes northwest and dips to the southwest, with local, short wavelength fluctuation on the surface trace. Because of its close location, similar trend, and similar slip sense to the aftershock belt, the Xiaoyudong fault has been proposed as a tear fault that accommodates the slip discrepancy on the major faults between the sub-segments (Li et al., 2009; Liu-Zeng et al., 2012) or the same structure as the NW-trending aftershock belts (Wang et al., 2015). However, the tear fault model is difficult to explain the slip sense of the Xiaoyudong fault. Located in the hanging-wall block of the JGF, the Xiaoyudong fault separates distinctive slip behaviors on the JGF. To its north, the JGF had ca. 1.5 m of co-seismic thrust slip during the Wenchuan earthquake; to the south, the JGF had little or no slip (Shen et al., 2009). Long-term activities on the JGF also show similar along-strike variations (Lu et al., 2014; Tan et al., 2017). If the Xiaoyudong fault were a tear fault that roots on the JGF, it would have had right-lateral sense-of-slip, in contrast with the observed sinistral-reverse co-seismic slip on the fault (Tan et al., 2012, 2017; Chang et al., 2012; Liu-Zeng et al., 2012; Chen et al., 2013). Therefore, we suggest that the Xiaoyudong fault is neither a tear fault on the JGF, nor the continuation of the NW-trending aftershock belts. This fault is likely a structure that absorbs the strain as the LTB builds up. The coincidence of the NW-SE strike direction of the fault and the aftershock belt may indicate the reactivation of crustal weak zones of similar trend in this region.

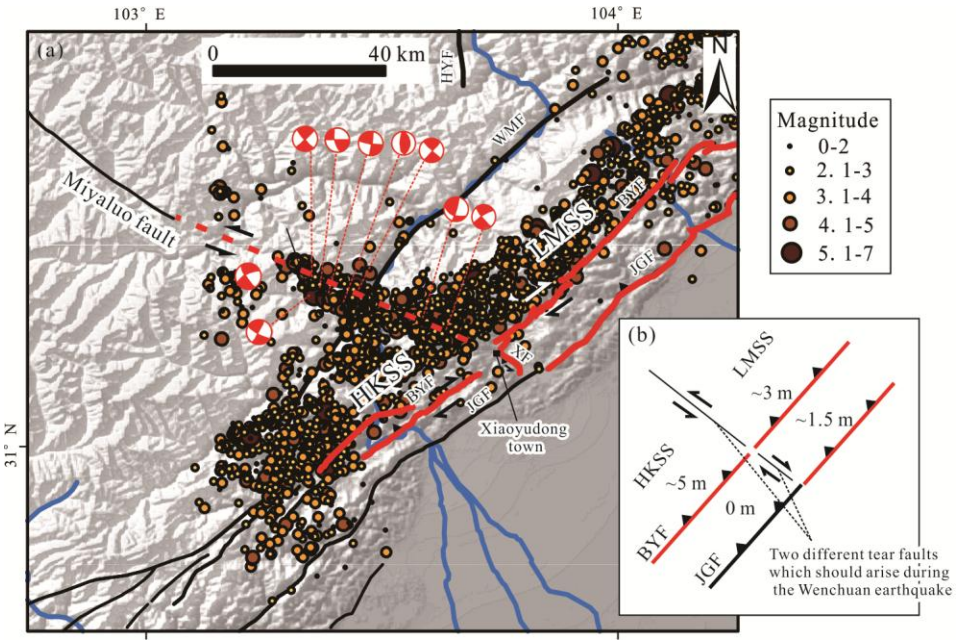

Figure 11. (a) Distribution of the aftershocks of the 2008 Wenchuan earthquake, featuring the northwest-trending aftershock belt with focal mechanism solutions for M_w>5 events (Hu et al., 2008). Major rivers in blue, active faults in black, and surface ruptures of the Wenchuan earthquake in red. (b) Simplified diagram showing the predicted dextral sense-of-slip of the Xiaoyudong fault, which is against the observed sinistral-reverse slip. The predicted sinistral sense-of-slip on the NW-trending aftershock belt is consistent with field and seismotectonic observations.

Conclusions

The central segment of the LTB is an ideal place to quantitatively understand the influences of external forces on orogenic processes, because its internal forces are largely identical along-strike whereas the external forces, as represented by the fluvial systems, vary remarkably along the mountain range. We have delineated the variations of the topography, fluvial incision intensity, co-seismic slips, and co-seismic landslides along the central LTB, and computed the compressional normal stresses on the major fault planes under the influence of the topography, which led us to the following findings:

(1) With similar boundary conditions of the internal (tectonic) forces, it is the lower fluvial incision intensity in the LMSS that results in the higher topography, which induces greater normal stresses on the fault planes, partially locking the existing thrust faults and promoting the slip

partitioning onto the JGF. Therefore, the along-strike variation of fluvial incision intensity in central LTB is the fundamental driver for the along-strike differences of topography and fault activities.

(2) The mean hillslope angle within the Pengguan massif, the hanging-wall block of the Beichuan-Yingxiu fault, had reached a threshold value of ca. 32 ° prior to the 2008 Wenchuan earthquake. Co-seismic deformation reduced the mean hillslope angle significantly, indicating that geomorphic indices may vary with different stages in an earthquake cycle. It is therefore promising to further study how landscape co-evolves with earthquake cycles, as it may shed light on seismic hazard assessment.

(3) The northwest-trending aftershock belt in the hinterland of the central LTB is a sinistral tear fault that results from the discordant fault slips on the BYF between the two sub-segments. In spite of its seemingly lateral continuation, we argue that the Xiaoyudong fault cannot be simply treated as another tear fault that roots on the JGF, because the slips on the JGF would require a dextral tear, rather than the observed sinistral-reverse slip on the fault.

Acknowledgements

This project has been fully supported by theNational Natural Science Foundation of China (41302159), the Special Projects for Basic Research Work of the Institute of Geology, China Earthquake Administration (IGCEA1518). The topography data (SRTM data V4) is from the website (http://srtm.csi.cgiar.org). The data of the fluvial shear stress is from Godard et al., 2010. The co-seismic thrust slip of the 2008 Wenchuan earthquake source from Shen et al., 2009. We thank Prof. Huiping Zhang, for his helpful suggestions which improved the manuscript.

References

Allen, P.A., 2009. Earth surface processes. John Wiley & Sons, 416 p.

Avouac, J.P. and Burov, E.B., 1996. Erosion as a driving mechanism of intracontinental mountain growth. *Journal of Geophysical Research: Solid Earth*, 101(B8): 17747-17769.

Beaumont, C., Fullsack, P. and Hamilton, J., 1992. Erosional control of active compressional

orogens. *Thrust tectonics*, 99, pp.1-18.

Beaumont, C., Jamieson, R.A., Nguyen, M.H., and Lee, B., 2001. Himalayan tectonics explained by extrusion of a low-viscosity crustal channel coupled to focused surface denudation. *Nature*, 414(6865): 738-742.

Bollinger, L., J. Avouac, R. Cattin, and M. Pandey, 2004. Stress buildup in the Himalaya, *Journal of Geophysical Research: Solid Earth*, *109*(B11).

Burbank D. W., J. Leland, E. Fielding, R. S. Anderson, N. Brozovic, M. R. Reid, and C. Duncan, 1996. Bedrock incision, rock uplift and threshold hillslopes in the northwestern Himalayas, *Nature* 379, 505-510.

Chang C., G. Chen, X. Xu, R. Yuan, Y. Kuo, and W. Chen, 2012. Influence of the pre-existing Xiaoyudong salient in surface rupture distribution of the Mw 7.9 Wenchuan earthquake, China, *Tectonophysics*, 530-531, 240–250.

Chen L., Y. Ran, H. Wang, X. Shi, R. Liu, and S. Dong, 2013. Paleoseismology and kinematic characteristics of the Xiaoyudong rupture, a short but significant strange segment characterized by the May 12, 2008, Mw 7.9 earthquake in Sichuan, China, *Tectonophysics*, 584, 91-101.

Chen, Y.-W., Shyu, J.B.H. and Chang, C.-P., 2015. Neotectonic characteristics along the eastern flank of the Central Range in the active Taiwan orogen inferred from fluvial channel morphology. *Tectonics*, 34, 2249-2270.

Chen Z., B. C. Burchfiel, Y. Liu, R. W. King, L. H. Royden, W. Tang, E. Wang, J. Zhao, and X . Zhang, 2000. Global Positioning System measurements from eastern Tibet and their implications for India/Eurasia intercontinental deformation, *J. Geophys. Res.*, 105, 16,215 – 16,227, doi:10.1029/2000JB900092.

Clark M, and L. H. Royden, 2000. Topographic ooze: building the eastern margin of Tibet by lower crustal flow. *Geology*, 28(8): 703～706.

Cui X., X. Hu, C. Yu, K. Tao, Y. Wang, and J. Ning, 2011. Research on Focal Mechanism Solutions of Wenchuan Earthquake Sequence. *Acta Scientiarum Naturalium Universitatis Pekinensis*, 47, (6), 1063-1072.

Dahlen, F.A., J. Suppe, and D. Davis, 1984. Mechanics of fold-and-thrust belts and accretionary wedges: Cohesive Coulomb theory. *Journal of Geophysical Research: Solid Earth*, 89(B12), pp.10087-10101.

560 Dahlen, F.A., and Suppe, J., 1988. Mechanics, growth, and erosion of mountain belts. *Geological*
561 *Society of America Special Papers*, 218, 161-178.
562 Dahlen, F.A., 1990. Critical taper model of fold-and-thrust belts and accretionary wedges. *Annual*
563 *Review of Earth and Planetary Sciences*, 18(1), pp.55-99.
564 Gao M., G. Zeilinger, X. Xu, X. Tan, Q. Wang, and M. Hao, 2016. Active tectonics evaluation from
565 geomorphic indices for the central and the southern Longmenshan range on the Eastern Tibtan
566 Plateau, China. *Tectonics*, doi: 10.1002/2015TC004080.
567 Gan W, P. Zhang, Z. K. Shen, Z. Niu, M. Wang, Y. Wan, D. Zhou, and J. Cheng, 2007. Present-
568 day crustal motion within the Tibetan Plateau. *J. Geophys. Res.* 112, B08416,
569 doi:10.1029/2005JB004120.
570 Godard, V., R. Pik, J. Lavé, R. Cattin, B. Tibari, J. de Sigoyer, M. Pubellier, and J. Zhu, 2009. Late
571 Cenozoic evolution of the central Longmen Shan, eastern Tibet: Insight from (U-Th)/He
572 thermochronometry, *Tectonics* 28, doi 10.1029/2008TC002407.
573 Godard V., J. Lavé, J. Carcaillet, R. Cattin, D. Bourlès, and J. Zhu, 2010. Spatial distribution of
574 denudation in Eastern Tibet and regressive erosion of plateau margins, *Tectonophysics*, 491,
575 253-274.
576 Howard A.D., W.E. Dietrich, and A. Seidl, 1994. Modeling fluvial erosion on regional to continental
577 scales. *J. Geophys. Res.* 99 (B7), 13971–13986.
578 Hu X. P., C. Q. Yu, K. Tao, X. F. Cui, J. Y. Ning, and Y. H. Wang, 2008. Fical mechanism solutions
579 of Wenchuan earthquake and its strong aftershocks obtained form initial P wave polarity
580 analysics. *Chinese J. Geophys.* (in Chinese), 51(6): 1711-1718.
581 Hua W., Z. L. Chen, and S. H. Zheng, 2009. A study on segmentation characteristics of aftershock
582 source parameters of Wenchuan earthquake in 2008. *Chinese J. Geophys.* (in Chinese), 52(2),
583 365-371.
584 Huang Y, J. P. Wu, T. Z. Zhang, and D. N. Zhang. Relocation of the M8.0 Wenchuan earthquake
585 and its aftershock sequence. *Science in China Series D: Earth Sciences*. 2008, 51(12):
586 1703~1711.
587 Jarvis A., H.I. Reuter, A. Nelson, and E. Guevara, 2008. Hole-filled seamless SRTM data V4,
588 International Centre for Tropical Agriculture (CIAT), available from http://srtm.csi.cgiar.org.
589 Jaupart, C., S. Labrosse, and J.-C., Mareschal, 2015. Temperatures, heat and energy in the mantle

590 of the earth. In: Gerald Schubert (editor-in-chief) Treatise on geophysics, 2nd edition, Vol 7.
591 Elsevier, p. 223-270.
592 Jiang Z., M. Wang, Y. Wang, Y. Wu, S. Che, Z. K. Shen, R. Burgmann, J. Sun, Y. Yang, H. Liao,
593 and Q. Li, 2013. GPS constrained coseismic source and slip distribution of the 2013 M_w6.6
594 Lushan, China, earthquake and its tectonic implications, *Geophys. Res. Lett.* 41, 407-413,
595 doi:10.1002/2013GL058812.
596 King, R. W., F. Shen, B. C. Burchfiel, L. H. Royden, E. Wang, Z. Chen, Y. Liu, X. Y. Zhang, J. X.
597 Zhao, and Y. Li, 1997. Geodetic measurements of crustal motion in southwest China, *Geology*,
598 25, 179 – 182, doi:10.1130/0091-7613.
599 Kirby, E., P. W. Reiners, M. A. Krol, K. X. Whipple, K. V. Hodges, K. A. Farley, W. Tang, and Z.
600 Chen, 2002. Late Cenozoic evolution of the eastern margin of the Tibetan Plateau: Inferences
601 from $^{40}Ar/^{39}Ar$ and (U-Th)/He thermochronology, *Tectonics* 21, doi 0.1029/2000TC001246.
602 Kirby E., K. Whipple, W. Tang and Z. Chen, 2003. Distribution of active rock uplift along the
603 eastern margin of the Tibetan Plateau: Inferences from bedrock channel longitudinal profiles,
604 *J. Geophys. Res.*108, B4, 2217, doi: 10.1029/2001JB000861.
605 Kirby E., K. Whipple, and N. Harkins, 2008. Topography reveals seismic hazard, *Nature Geoscience*,
606 1, 485-487.
607 Li, Y., L.Q. Huang, A.L. Densmore, R.J. Zhou, L.Yan, Y. Zhang, N. Richardson, S.L. Dong, B.C.
608 Qiao, M.A. Ellis, Y.L. He, H. Chen, and B.L. Ma, 2009. Surface rupture of Xiaoyudong fault
609 caused by Wenchuan earthquake and its geological significance. *Quaternary Sciences* 29, 502-
610 512 (in Chinese).
611 Li Z. X., J. Wartho, S. Occhipinti, C. Zhang, X. Li, J. Wang, and C. Bao, 2007. Early history of the
612 eastern Sibao Orogen (South China) during the assembly of Rodinia: New mica 40Ar/39Ar
613 dating and SHRIMP U–Pb detrital zircon provenance constraints, *Precambrian*
614 *Research* , 159 (1–2) :79-94.
615 Liang, S., Gan,W., Shen, C., Xiao, G., Liu, J., Chen,W., Ding, X., Zhou, D., 2013. Three-
616 dimensional velocity field of present-day crustal motion of the Tibetan Plateau derived from
617 GPS measurements. J. Geophys. Res. Solid Earth 118:1 – 11.
618 http://dx.doi.org/10.1002/2013JB010503.
619 Liu-Zeng J., Z. Zhang, L. Wen, P. Tapponnier, J. Sun, X. Xing, G. Hu, Q. Xu, L. Zeng, L. Ding, C.

Ji. K. W. Hudnut, and J. van der Woerd, 2009. Co-seismic ruptures of the 12 May 2008, M_s 8.0 Wenchuan earthquake, Sichuan: East-west crustal shortening on oblique, parallel thrusts along the eastern edge of Tibet, *Earth and Planetary Science Letters* 286: 355-370.

Liu-Zeng J., L. Wen, M. Oskin, and L. Zeng, 2011. Focused modern denudation of the Longmen Shan margin, eastern Tibetan Plateau, *Geochem. Geophys. Geosyst.*, 12, Q11007, doi:10.1029/2011GC003652.

Liu-Zeng J., J. Sun, P. Wang, K. Ww. Hudnut, C. Ji, Z. Zhang, Q. Xu, L. Wen, 2012. Surface ruptures on the transverse Xiaoyudong fault: A significant segment boundary breached during the 2008 Wenchuan earthquake, China. *Tectonophysics*, 580: 218-241.

Liu, L. Z., and D. Mark, 1992. The effect of topography on the state of stress in the crust: Application to the site of the Cajon Pass Scientific Drilling Project, *Journal of Geophysical Research*, 97(B4), 5095-5108, doi:10.1029/91JB01355.

Liu, S.G., Z.L. Luo, S.L. Dai, A. Dennis, and C.J.L. Wilson, 1996. The uplift of the Longmenshan thrust belt and subsidence of the West Sichuan Foreland Basin. *Acta Geol. Sin. Engl. Ed.* 9 (1), 16 – 26.

Lu R., D. He, J. Suppe, Y. Ma, B. Liu, and Y. Chen, 2012. Along-strike variation of the frontal zone structural geometry of the Central Longmen Shan thrust belt revealed by seismic reflection profiles, *Tectonophysics*, 580, 178-191.

Lu R., D. He, S. John, J. E. Wu, B. Liu, and Y. Chen, 2014, Structural model of the central Longmen Shan thrusts using seismic reflection profiles: Implications for the sediments and deformations since the Mesozoic, *Tectonophysics*, 630, 43-53.

Luttrell, K. M., X. Tong, D. T. Sandwell, B. A. Brooks, and M. G. Bevis, 2011. Estimates of stress drop and crustal tectonic stress from the 27 February 2010 Maule, Chile, earthquake: Implications for fault strength, *Journal of Geophysical Research: Solid Earth*, 116(B11).

Ma, Y.W., and J. Yang, 2001. Tectonic deformation of the nappe tectonic in the middle Longmen Mountains (in Chinese with English abstract). *J. Chengdu Univ. Technol.* 28 (3), 236 – 241.

Meade B. J., C. P. Conrad, 2008. Andean growth and the deceleration of South American subduction: Time evolution of a coupled orogen-subduction system, *Earth and Planetary Science Letters*, 275(1): 93-101.

Mugnier, J.L., Baby, P., Colletta, B., Vinour, P., Bale, P., and Leturmy, P., 1997. Thrust geometry

650 controlled by erosion and sedimentation: A view from analogue models. Geology, 25(5), 427-
651 430.
652 Molnar, P. and England, P., 1990. Late Cenozoic uplift of mountain ranges and global climate change:
653 chicken or egg? *Nature*, 346(6279): 29-34.
654 Oskin, M.E., Arrowsmith, J.R., Corona, A.H., Elliott, A., Fletcher, J.M., Fielding, E.J., Gold, P.O.,
655 Garcia, J., Hudnut, K.W., Liu-Zeng, J., Teran, O., 2012. Near-field deformation from the EI
656 Mayer-Cucapah earthquake revealed by differential LiDAR. *Science* 335, 702 – 705.
657 Parker R. N., A. L. Densmore, N. J. Rosser, M. de Michele, Y. Li, R. Huang, S. Whadcoat, and D.
658 N. Petley, 2011. Mass wasting triggered by the 2008 Wenchuan earthquake is greater than
659 orogenic growth, *Nature Geoscience* 4, 449-452.
660 Ran, Y., L. Chen, J. Chen, H. Wang, G. Chen, J. Yin, X. Shi, C. Li, and X. Xu, 2010. Paleoseismic
661 evidence and repeat time of large earthquakes at three sites along the Longmenshan fault zone.
662 *Tectonophysics* 491, 141-153.
663 Ren Z., Z. Zhang, F. Dai, J. Yin, and H. Zhang, 2014. Topographic changes due to the 2008 Mw 7.9
664 Wenchuan earthquake as revealed by the differential DEM method, *Geomorphology* 217, 122-
665 130.
666 Roger, F., M., Jolivet, and J., Malavieille, 2010. The tectonic evolution of the Songpan-Garze (north
667 Tibet) and adjacent areas from Proterozoic to present: A synthesis. *Journal of Asian Earth*
668 *Sciences*, v. 39, p. 254 – 269, doi: 10 .1016/j .jseaes .2010 .03 .008.
669 Shen Z. K, J. Sun, P. Zhang, Y. Wan, M. Wang, R. Burgmann, Y. Zeng, W. Gan, H. Liao, and Q.
670 Wang, 2009. Slip maxima at fault junctions and rupturing of barriers during the 2008
671 Wenchuan earthquake, *Nature Geoscience*, doi: 10.1038/NGEO636.
672 Steer, P., Simoes, M., Cattin, R. and Shyu, J.B.H., 2014. Erosion influences the seismicity of active
673 thrust faults. *Nature Communication*, 5, 5564, doi:10.1038/ncomms6564.
674 Styron, R. H., and E. A. Hetland, 2015. The weight of the mountains: Constraints on tectonic stress,
675 friction, and fluid pressure in the 2008 Wenchuan earthquake from estimates of topographic
676 loading, *Journal of Geophysical Research: Solid Earth*, 120(4), 2697-2716.
677 Sun C., D. Jia, H. Yin, Z. Chen, Z. Li, L. Shen, D. Wei, Y. Li, B. Yan, M. Wang, S. Fang, and J. Cui.
678 2016. Sandbox modeling of evolving thrust wedges with different preexisting topographic
679 relief: Implications for the Longmen Shan thrust belt, eastern Tibet. *Journal of Geophysical*

Research: Solid Earth, doi: 10.1002/2016JB013013.

Tackley, P.J., 2000. Mantle convection and plate tectonics: toward an integrated physical and chemical theory. Science, 288(5473), pp.2002-2007.

Tan, X., R. Yuan, X. Xu, G. Chen, Y. Klinger, C. Chang, J. Ren, C. Xu, and K. Li, 2012. Complex surface rupturing and related formation mechanisms in the Xiaoyudong area for the 2008 Mw 7.9 Wenchuan Earthquake, China, *J. Asian Earth Sci.*, 58, 132–142, doi:10.1016/j.jseaes.2012.06.005.

Tan X., X. Xu, and R. Lu, 2017a. Comment on "Sandbox modeling of evolving thrust wedges with different preexisting topographic relief: Implications for the Longmen Shan thrust belt, eastern Tibet" by C. Sun et al. *Journal of Geophysical Research: Solid Earth*, doi: 10.1002/2016JB013505.

Tan X. B., X. W. Xu, Y. H. Lee, R. Q. Lu, Y. Liu, C. Xu, K. Li, G. H. Yu, and W. J. Kang, 2017b. Late Cenozoic thrusting of major faults along the central segment of Longmen Shan, eastern Tibet: Evidence from low-temperature thermochronology. *Tectonophysics* 712-713: 145-155.

Wang, E., E. Kirby, K.P. Furlong, M. van Soest, G. Xu, X. Shi, P.J.J. Kamp, and K.V. Hodges, 2012. Two-phase growth of high topography in eastern Tibet during the Cenozoic, *Nat. Geos.*, doi: 10.1038/NGEO1538.

Wang, P., Scherler, D., Liu-Zeng, J., Mey, J., Avouac, J., Zhang, Y., and Shi, D., Tectonic control of Yarlung Tsangpo Gorge revealed by a buried canyon in Southern Tibet. *Science*, 2014. 346(6212): 978-981.

Wan, Y., Z.-K. Shen, R. Bürgmann, J. Sun, and M. Wang, 2017. Fault geometry and slip distribution of the 2008 Mw 7.9 Wenchuan, China earthquake, inferred from GPS and InSAR measurements, *Geophysical Journal International*, 208(2): 748-766.

Wang W. M., L. F. Zhao, J. Li, and Z. X. Yao, 2008. Rupture process of the M_s8.0 Wenchuan earthquake of Sichuan , China. *Chinese J. Geophys.* (in Chinese), 51(5):1403-1410.

Wang W. M., J. L. Hao, and Z.X. Yao, 2013. Preliminary result for rupture process of Apr. 20, 2013, Lushan Earthquake, Sichuan, China. *Chinese J. Geophys*, (in Chinese), 56(4):1412-1417, doi:10.6038/cjg20130436.

Wang W., Y. Qing, C. Zhu, X. Shan, and X. Zhang, 2015. Geological characteristics of transverse faults and its earthquake-controlling function along the Longmenshan fault zone. *Journal of*

710 *Seismological Research*, (in Chinese) 38(2), 242-249.
711 Wang W., V. Godard, J. Liu-Zeng, D. Scherler, C. Xu, J. Zhang, K. Xie, O. Beller, C. Ansberque, J.
712 de Sigiyer, and A.S.T.E.R Team, 2017. Perturbation of fluvial sedment fluxes following the
713 2008 Wenchuan earthquake. *Earth Surface Processes and Landforms*. Doi:10.1002/esp.4210.
714 Whipple, K.X., and B.J. Meade , 2004. Controls on the strength of coupling among climate, erosion,
715 and deformation in two-sided, frictional orogenic wedges at steady state. *J. Geophys. Res.* 109,
716 F01011.
717 Willett S. D., 1999. Rheological dependence of extension in wedge models of convergent orogens.
718 *Tectonophysics* 305:419-435.
719 Willett S.D., and M.T. Brandon, 2002. On steady states in mountain belts. *Geology* 30, 175 – 178.
720 Wu J. P., Y. Huang, T. Z. Zhang, Y. H. Ming, and L. H. Fang, 2009. Aftershock distribution of the
721 Ms8.0 Wenchuan earthquake and 3-D P-wave velocity structure in and around source region,
722 *Chinese J. Geophys.*, (in Chinese), 52(1), 102~111.
723 Xu C, X. Xu, X. Yao, and F. Dai, 2014. Three (nearly) complete inventories of landslides triggered
724 by the May 12, 2008 Wenchuan M_w 7.9 earthquake of China and their spatial distribution
725 statistical analysis. *Landslides* 11(3): 441-461.
726 Xu C., X. Xu, L. Shen, Q. Yao, X. Tan, W. Kang, S. Ma, X. Wu, J. Cai, M. Gao, and K., Li, 2016.
727 Optimized volume models of earthquake-triggered landslides. *Scientific Reports* 6: 29797.
728 Xu, X., X. Wen, G. Yu, G. Chen, Y. Klinger, J. Hubbard, and J. H. Shaw, 2009. Coseismic reverse-
729 and oblique-slip surface faulting generated by the 2008 Mw 7.9 Wenchuan earthquake, China,
730 *Geology* 27, 515–518.
731 Xu Y.-G., B. He, S.-L. Chung, M. A. Menzies, and F. A. Frey, 2004. Geologic, geochemical, and
732 geophysical consequences of plume involvement in the Emeishan flood-basalt province,
733 *Geology*, 32, 10, 917-920.
734 Yi G. X., F. Long, and Z. W., Zhang, 2012. Spatial and temporal variation of focal mechannisms for
735 aftershocks of the 2008 Ms8.0 Wenchan earthquake. *Chinese J. Geophys.* (in Chinese),
736 55(4):1213-1227.
737 Yu G., X. Xu, Y. Klinger, G. Diao, G. Chen, X. Feng, C. Li, A. Zhu, R. Yuan, T. Guo, X. Sun, X.
738 Tan, and Y. An, 2010. Fault-Scarp features and Cascading-Ropture Model for the Wenchuan
739 Earthquake (M_w 7.9), Eastern Tibetan Plateau, China. *Bulletin of the Seismological Society of*

America 100(5B). doi: 10.1785/0120090255.

Yue H., Z. E. Ross, C. Liang, S. Michel, H. Fattachi, E. Fielding, A. Moore, Z. Liu, and B. Jia, 2017. The 2016 Kumamoto Mw = 7.0 earthquake: a significant event in a fault-volcano system. *Journal of Geophysical Research: Solid Earth*, under review.

Zeitler, P.K., P.O. Koons, M.P. Bishop, C.P. Chamberlain, D. Craw, M.A. Edwards, S. Hamidullah, M.Q. Jan, M.A. Khan, M.U.K. Khattak, W.S.F. Kidd, R.L. Mackie, A.S. Meltzer, S.K. Park, A. Pecher, M.A. Poage, G. Sarker, D.A. Schneider, L. Seeber, and J.F. Shroder, 2001. Crustal reworking at Nanga Parbat, Pakistan: Metamorphic consequences of thermal-mechanical coupling facilitated by erosion. *Tectonics*, 20(5): 712-728.

Zeitler P. K., P.O. Koons, B. Hallet, and A.S. Meltzer, 2015. Comment on "Tectonic control of Yarlung Tsangpo Gorge revealed by a buried canyon in Southern Tibet". *Science*, 349(6250): 799.

Zhang H., P. Zhang, E. Kirby, J. Yin, C. Liu, and G. Yu, 2011. Along-strike topographic variation of the Longmen Shan and its significance for landscape evolution along the eastern Tibetan Plateau. *Journal of Asian Earth Sciences* 40, 855-864.

Zhang H. P., M.E. Oskin, J. Liu-Zeng, P. Zhang, P. W. Reiners, and P. Xiao, 2016. Pulsed exhumation of interior eastern Tibet: Implications for relief generation mechanisms and the origin of high-elevation planation surfaces, *Earth and Planetary Science Letters*, 449 :176-185

Zhang, P. Z., 2013, A review on active tectonics and deep crustal processes of the Western Sichuan region, eastern margin of the Tibetan Plateau, *Tectonophysics*, 584, 7–22, doi:10.1016/j.tecto.2012.02.021.

Zhang, Z., X. Yuan, Y. Chen, X. Tian, R. Kind, X. Li, and J. Teng, 2010. Seismic signature of the collision between the east Tibetan escape flow and the Sichuan Basin. *Earth and Planetary Science Letters* 292, 54–264.

Zheng G., H. Wang, T. J. Wright, Y. Lou, R. Zhang, W. Zhang, C. Shi, J. Huang, and N. Wei, 2017. Crustal deformation in the India-Eurasia collision zone from 25 years of GPS measrements. *Journal of Geophysical Research: Solid Earth*, doi: 10.1002/2017JB014465.